Coarse-grained dynamics in quantum many-body systems using the maximum entropy principle

Adán Castillo,[1] Carlos Pineda,[2,*] Erick Sebastián Navarrete,[3,2] and David Davalos[4,5]

[1]*Faculté de Physique et Ingénierie, Université de Strasbourg, 3-5 Rue de l'Université, Strasbourg 67084, France*
[2]*Instituto de Física, Universidad Nacional Autónoma de México, Ciudad de México 01000, Mexico*
[3]*Facultad de Ciencias, Universidad Nacional Autónoma de México, Ciudad de México 01000, Mexico*
[4]*Institute of Physics, Slovak Academy of Sciences, Dúbravská Cesta 9, Bratislava 84511, Slovakia*
[5]*Departamento de Física, Universidad de Guadalajara, Guadalajara, Jalisco 44430, Mexico*

(Received 3 April 2025; accepted 22 July 2025; published 2 September 2025)

Starting from a coarse-grained map of a quantum many-body system, we construct the inverse map that assigns a microscopic state to a coarse-grained state based on the maximum entropy principle. Assuming unitary evolution in the microscopic system, we examine the resulting dynamics in the coarse-grained system using the assignment map. We investigate both a two-qubit system, with SWAP and controlled-NOT gates, and n-qubit systems, configured either in an Ising spin chain or with all-to-all interactions. We demonstrate that these dynamics exhibit atypical quantum behavior, such as nonlinearity and non-Markovianity. Furthermore, we find that these dynamics depend on the initial coarse-grained state and establish conditions for general microscopic dynamics under which linearity is preserved. As the effective dynamics induced by our coarse-grained description of many-body quantum systems diverge from conventional quantum behavior, we anticipate that this approach could aid in describing the quantum-to-classical transition and provide deeper insights into the effects of coarse graining on quantum systems.

DOI: 10.1103/shy4-8h5g

I. INTRODUCTION

Coarse-grained descriptions have been extensively used to study quantum systems [1–10]. This type of effective modeling is essential because the full quantum description is usually impractical as the Hilbert space dimension grows exponentially with respect to the number of particles. In this regard, coarse graining is generally implemented by reducing the number of degrees of freedom; however, the way this is done is not unique [11]. Moreover, coarse graining has been pivotal in studying the quantum-to-classical transition [1,12], which remains, along with the measurement problem, an active area of research due to the inherent linearity of the theory and the mathematical connections between the studied entities and the outcomes of measurement [13–15]. It has been employed also in the study of the thermalization of closed quantum systems [16,17].

Using the language of quantum information, several authors have introduced the concept of coarse graining in the quantum realm. In Ref. [11] coarse graining was defined via classical stochastic maps between measures defined using quantum observables; in Ref. [18] a framework exploiting Stinespring dilation [19] was introduced to keep track of the information dumped. Both frameworks accommodate a variety of coarse-graining maps. A class of quantum channels, amounting to a coarse-grained description of many-body systems, was introduced in [20]. A key feature in common is that the coarse-grained description contains less information than the original fine-grained picture.

A natural and fundamental question concerns how a physical system appears when probed with imperfect measurement devices. This issue is of central importance, as all experimental observations are inherently limited by some degree of imprecision. Such limitations raise critical concerns about the implications they may have on the information extracted from a system. In special relativity, for example, the behavior of rods and clocks plays a key role in defining foundational concepts such as simultaneity [21], while in quantum mechanics, the von Neumann postulate establishes the framework for what can be observed and how [22]. In the context of quantum states, it has been shown that the space of observable states shrinks doubly exponentially as a result of finite addressing errors [20]. Of particular interest, both fundamentally and practically, is the question of how the dynamics of many-body quantum systems appears through the lens of imperfect measurements. The limitations introduced by such coarse-grained observations must be carefully considered when analyzing and interpreting the evolution of complex quantum systems.

This question has been addressed from several points of view. There have been efforts to define and investigate the dynamics governing coarse-grained descriptions of quantum systems. For example, in Ref. [18] the impact on the emerging dynamics due to the choice of the fine-grained state was discussed. In Refs. [23,24] two ways of assigning fine-grained quantum states were analyzed for the blurred detector across various assignment maps. The key result in these works is the emergence of nonlinear and non-Markovian dynamics. We believe that a deeper exploration of such results is needed,

*Contact author: carlospgmat03@gmail.com

especially in the context of many-body systems under general but tractable enough assumptions.

In this work we address this need by exploring coarse-grained descriptions of many-body quantum systems and the emergent dynamics using the idea of assignment map [23,24] to "invert" the coarse-graining map. Two crucial objects must be chosen carefully to achieve our goal. First, we need a general enough coarse-graining map to accommodate a decent variety of many-body systems. To do this, we consider a recently developed coarse-grained model [20], which is based on particle-indexing noise and a reduction of the number of particles. More specifically, this model assumes that when a measurement is performed, possibly involving multiple particles, the subset of particles being measured can vary randomly. This coarse-graining approach has two key features that make it relevant for further study. First, it captures the limitations of a measurement device that cannot resolve individual particles, resembling the behavior of a macroscopic apparatus observing a quantum system. Potentially, this can contribute to a better understanding of the quantum-to-classical transition. Second, the model allows for the exploration of how different spatial configurations influence quantum states. It can incorporate various geometries, such as linear chains (see, e.g., [25,26]), two-dimensional lattices (see, e.g., [27,28]), or more complex layouts like those found in IBM quantum processors (see, e.g., [29]).

Second, we must choose an assignment map. There is a variety of criteria for selecting one. In Ref. [24] the authors analyzed the difference between two assignment maps, one on them based on the maximum entropy (MaxEnt) principle and the other based on the average compatible pure states. The MaxEnt principle serves as a method of inference that assigns probabilities to all events while ensuring compatibility with the known information, given as expectation values. The resulting distribution is the least biased, i.e., it maximizes the entropy [30]. The role of the MaxEnt principle as an inference method in the formulation of statistical mechanics ensembles for general observables was thoroughly discussed in Jaynes' widely cited paper [31]. This work extends beyond the canonical and microcanonical ensembles, providing a more general framework. Its application to the quantum realm was further developed in a subsequent paper [32] (see also [33]). In the quantum case, the measure of uncertainty is the von Neumann entropy and the resulting probability distribution (or density matrix, in the quantum case) reflects these values without introducing any additional information. It is worth mentioning that this principle has been used for tackling the lack of information in other scenarios, for example, in incomplete state (and process) quantum tomography [34–36]. We have chosen MaxEnt to construct the assignment map compatible with the coarse-graining map for both its solid physical motivation, in terms of information, and the fact that it is analytically convenient.

Having established the connection between both scales using the aforementioned maps, we investigate the emergent coarse-grained dynamics induced by various quantum dynamics at the finer scale. Specifically, we assume that only the coarse-grained scale is accessible, meaning that expectation values are expressed in terms of operators at this scale. Consequently, we construct the corresponding operators at the finer scale such that they reproduce the same expectation values while simultaneously encoding the coarse-graining map. With these elements in place, we formulate the MaxEnt states required for the assignment map. Finally, the emergent coarse-grained dynamics naturally arise as the concatenation of the coarse-graining maps and the dynamics at the finer scale. We consider examples of both small and large many-body quantum systems.

The paper is organized as follows. In Sec. II we introduce both the coarse-graining map and the maximum entropy assignment map, and with these elements we proceed to construct the effective dynamics of the macroscopic system. Then we apply these tools to different quantum dynamical systems. In particular, Sec. III is devoted to the study of the effective dynamics of a two-qubit system with underlying SWAP and controlled-NOT gates. In Sec. IV we explore the effective dynamics of an n-qubit system configured as an Ising spin chain, with both all-to-all and nearest-neighbor interactions. In Sec. V we establish conditions for general microscopic dynamics under which linearity is preserved, and we present an example of a microscopic dynamics that preserves linearity but is nonetheless non-Markovian. We summarize our work and discuss our conclusions in Sec. VI.

II. EFFECTIVE DYNAMICS IN COARSE-GRAINED SYSTEMS

In this section we introduce the coarse-graining map from which the effective description of the state is recovered. We construct the maximum entropy assignment map that will be used to assign a microscopic state to the effective state and study some of its properties. This map is used to formally present the effective dynamics in a quantum many-body system subject to a coarse-grained description.

A. Coarse-graining map

Consider an imperfect measuring device that is subject to two types of errors. First, the device lacks the capability to accurately distinguish between the individual particles of a d-level n-body system. In other words, there exists a nonzero probability p_P of wrongly identifying particles according to a permutation P. This type of measurement is referred to as a fuzzy measurement. Second, the device does not have the ability to resolve all particles; only a subset τ of m particles can be measured. Mathematically, a partial trace over the complement of τ is performed. A coarse-grained description of the system is obtained when both types of error are combined [20], in the sense that expected values should be calculated with respect to an effective state resulting from the application of the coarse-graining map

$$\mathcal{C} : \mathcal{B}\left(\mathsf{H}_d^{\otimes n}\right) \to \mathcal{B}\left(\mathsf{H}_d^{\otimes m}\right), \quad \varrho \mapsto \mathrm{tr}_{\bar{\tau}}\left(\sum_P p_P P(\varrho)\right), \tag{1}$$

where $\mathrm{tr}_{\bar{\tau}}$ represents the partial trace over the complement of τ and $\mathcal{B}(\mathsf{H})$ is the space of bounded linear operators acting on H.

Our primary focus is directed towards a particular case of the coarse-graining map given by (1). First, the measuring device might mistakenly swap pairs of particles. Second, it is

able to resolve a single particle, that is, $m = 1$. Without loss of generality, we can assume that the first particle is the one that is intended to be measured, so that $\tau = 1$. The coarse-graining map that captures this situation is

$$\mathcal{C} : \mathcal{B}\left(\mathsf{H}_d^{\otimes n}\right) \to \mathcal{B}(\mathsf{H}_d), \quad \varrho \mapsto \mathrm{tr}_{\bar{1}}\left(\sum_k p_k P_{1,k}(\varrho)\right), \tag{2}$$

where $P_{1,k}$ is the permutation between the first and the kth particle and $P_{1,1} \equiv \mathbb{1}$. If state tomography were to be performed on the system using our imperfect apparatus, the result would be a one-particle effective state $\rho_{\mathrm{eff}} = \mathcal{C}(\varrho)$; similarly, the expected value of any single-particle observable A will be $\mathrm{tr}[A\mathcal{C}(\varrho)]$. It is crucial to recognize that the resulting effective state is a mixture of all the reduced systems of the microscopic system (assuming $p_k \neq 0 \,\forall\, k$).

Two specific probability distributions p_k hold particular significance in this context:

$$p_k = \frac{1}{n} \,\forall\, k, \quad p_k = \frac{1 - p_1}{1 - n} \,\forall\, k \neq 1. \tag{3}$$

The first one represents the scenario in which the measuring device is completely incapable of distinguishing between the individual particles. This situation is akin to a gas, where each particle has an equal probability of being found anywhere within the system. The second one can be interpreted as the first particle being the one that is closest to the measuring device and the other providing a mean background noise. These distributions are referred to as nonpreferential and preferential distributions, respectively.

B. Maximum entropy principle and assignment map

Now let us shift our attention to the assignment map, which allows us to make an inference about the microscopic state of the system through our coarse-grained measurements. It is through this map that we will be able to obtain the state that will evolve according to the microscopic dynamics. The assignment map is constructed by selecting the microscopic state that maximizes the von Neumann entropy, while ensuring that it corresponds to the effective macroscopic state under a specific coarse-graining map, in a similar spirit as in [31,37] or in the context of coarse graining [18,24]. The maximization of entropy is carried out using the method of Lagrange multipliers, where the information of the effective state will be used as constraints.

Let us assume that we are able to perform state tomography on the effective state [38]. If $\{\varsigma^\alpha\}_\alpha$ is a tomographically complete set of operators acting on the Hilbert space H_d of the effective state $\mathcal{C}(\varrho)$, then its expected values can be connected to the expected values of a set of operators $\{G^\alpha\}_\alpha$ acting on the Hilbert space of the microscopic state, $\mathsf{H}_d^{\otimes n}$. These operators are defined by

$$G^\alpha = \sum_{k=1}^{n} p_k \varsigma_k^\alpha, \tag{4}$$

where ς_k^α is the operator ς^α acting on the kth particle. This connection is expressed mathematically by

$$\mathrm{tr}(\varsigma^\alpha \rho_{\mathrm{eff}}) = \mathrm{tr}(G^\alpha \varrho) \tag{5}$$

and is studied in Appendix A. Notice that the operators G^α can be thought of as fuzzy operators since they are equivalent to applying the ς^α operator to the kth particle with probability p_k. Note that the set $\{G^\alpha\}_\alpha$ is not tomographically complete, implying that we do not have access to all the details about the microscopic system.

Given the expected values of the G^α operators, the state that maximizes the von Neumann entropy is then [33]

$$\varrho_{\max} = \frac{1}{Z} \exp\left(\sum_{k=1}^{n} p_k \sum_{\alpha=1}^{d^2-1} \lambda_\alpha \varsigma_k^\alpha\right), \tag{6}$$

where λ_α is the Lagrange multiplier associated with the expectation value $\mathrm{tr}(\varsigma^\alpha \rho_{\mathrm{eff}})$. Indeed,

$$\mathrm{tr}(\varsigma^\alpha \rho_{\mathrm{eff}}) = \frac{\partial}{\partial \lambda_\alpha} \ln(Z), \tag{7}$$

with the partition function

$$Z = \mathrm{tr}\left[\exp\left(\sum_{\alpha=1}^{d^2-1} \lambda_\alpha G^\alpha\right)\right]. \tag{8}$$

Because the operators $p_k \sum_\alpha \lambda_\alpha \varsigma_k^\alpha$ in Eq. (6) commute, it is easy to observe that the maximum entropy state is separable. Due to this property, the maximum entropy assignment map is

$$\mathcal{A}_{\mathcal{C}}^{\max} : \mathcal{S}(\mathsf{H}_d) \to \mathcal{S}\left(\mathsf{H}_d^{\otimes n}\right),$$
$$\rho_{\mathrm{eff}} \mapsto \bigotimes_{k=1}^{n} \frac{1}{Z_k} \exp\left(p_k \sum_{\alpha=1}^{d^2-1} \lambda_\alpha \varsigma^\alpha\right), \tag{9}$$

where Z_k is the partition function associated with the kth particle and $\mathcal{S}(\mathsf{H})$ is the set of density matrices acting on H. The dependence of the assigned state on the effective state is encoded in the λ_α parameters. In fact, given the effective state ρ_{eff}, the λ_α parameters are obtained by noting that the norm of the generalized Bloch vector of the effective state, $\vec{r}_{\mathrm{eff}} = r_{\mathrm{eff}} \hat{n}_{\mathrm{eff}}$, can be expressed as

$$r_{\mathrm{eff}} = \sum_{k=1}^{n} p_k r_k, \tag{10}$$

where

$$r_k = \tanh(p_k \lambda), \quad \lambda = \left(\sum_\alpha \lambda_\alpha^2\right)^{1/2}. \tag{11}$$

Thus, inverting (10), we can find all the λ_α parameters from $\vec{r}_{\mathrm{eff}}$. More precisely,

$$\lambda_\alpha = \frac{r_{\mathrm{eff}}^\alpha}{r_{\mathrm{eff}}} \lambda, \tag{12}$$

where r_{eff}^α is the α component of the $\vec{r}_{\mathrm{eff}}$ Bloch vector. Now the assigned states by the maximum entropy assignment map in the preferential and nonpreferential cases (3) are

$$\mathcal{A}_{\mathcal{C}}^{\max}(\rho_{\mathrm{eff}}) = \rho_1 \otimes \rho_{\mathrm{np}}^{\otimes(n-1)}, \tag{13}$$
$$\mathcal{A}_{\mathcal{C}}^{\max}(\rho_{\mathrm{eff}}) = \rho_{\mathrm{eff}}^{\otimes n}, \tag{14}$$

respectively. In the preferential case (13), we have defined the reduced state of the nonpreferential particles as

$$\rho_{\mathrm{np}} = \frac{1}{Z_{\mathrm{np}}} \exp\left(\frac{1-p_1}{n-1} \sum_{\alpha=1}^{d^2-1} \lambda_\alpha \sigma^\alpha \right). \tag{15}$$

Noticeably, the assignment map $\mathcal{A}_{\mathcal{C}}^{\max}$ is clearly nonlinear [see Eq. (14)]. As an example, consider the nonpreferential case with the state $\mathbb{1}/2$; we have $\mathcal{A}_{\mathcal{C}}^{\max}(\mathbb{1}/2) = \mathbb{1}/2 \otimes \mathbb{1}/2 = \mathbb{1}/4$, which is not equal to $\mathcal{A}_{\mathcal{C}}^{\max}(|0\rangle\langle 0|)/2 + \mathcal{A}_{\mathcal{C}}^{\max}(|1\rangle\langle 1|)/2 = |00\rangle\langle 00|/2 + |11\rangle\langle 11|/2$. Also observe that $\mathcal{A}_{\mathcal{C}}^{\max}$ is defined once $\mathcal{C}$ is given such that their interplay is

$$\mathcal{C} \circ \mathcal{A}_{\mathcal{C}}^{\max} = \mathrm{id}_{\mathcal{S}(\mathsf{H}_d)}, \tag{16}$$

where the map $\mathrm{id}_{\mathcal{S}(\mathsf{H}_d)}$ is an affine mapping and has a unique linear extension on $\mathcal{B}(\mathsf{H}_d)$ [11], namely, $\mathrm{id}_{\mathcal{B}(\mathsf{H}_d)}$. This is relevant because, as we will show later, the emergent effective dynamics is generally nonlinear. The nonlinearity will come from the interplay of $\mathcal{C}$ and $\mathcal{A}_{\mathcal{C}}^{\max}$, with the microscopic dynamics, where the only element that is nonlinear is $\mathcal{A}_{\mathcal{C}}^{\max}$ alone.

C. Effective dynamics

Now that we have established the use of a coarse-graining model that incorporates both resolution and permutation errors and have constructed an assignment map based on the maximum entropy principle, we can explore the evolution of the effective system. Since we assume that the state that propagates due to the underlying evolution is precisely the one assigned via the maximum entropy assignment map, we can represent the dynamics of the effective state through the commutative diagram

$$\begin{array}{ccc} \rho_{\mathrm{eff}}(0) & \xmapsto{\Gamma_t} & \rho_{\mathrm{eff}}(t) \\ \Big\downarrow{\scriptstyle \mathcal{A}_{\mathcal{C}}^{\max}} & & \Big\uparrow{\scriptstyle \mathcal{C}} \\ \varrho_{\max}(0) & \xmapsto[\mathcal{V}_t]{} & \varrho_{\max}(t), \end{array}$$

where $\mathcal{V}_t$ is the evolution of the microscopic state. The evolution of the effective state Γ_t can be thus obtained from the composition three different operations [23]. First, a microscopic state is assigned to the effective state through the MaxEnt assignment map. Then the assigned map is propagated via $\mathcal{V}_t$. Finally, we define the coarse-grained description of the evolved assigned state to be the evolved effective state. In this way, we define the coarse-grained dynamics as the composition

$$\Gamma_t : \mathcal{S}(\mathsf{H}_d) \to \mathcal{S}(\mathsf{H}_d), \quad \rho_{\mathrm{eff}} \mapsto \left(\mathcal{C} \circ \mathcal{V}_t \circ \mathcal{A}_{\mathcal{C}}^{\max}\right)(\rho_{\mathrm{eff}}). \tag{17}$$

As mentioned above, while $\mathcal{C} \circ \mathcal{A}_{\mathcal{C}}^{\max}$ admits the identity map as a linear extension on $\mathcal{B}(\mathsf{H}_d)$, this linearity is generally broken in the full composition $\mathcal{C} \circ \mathcal{V}_t \circ \mathcal{A}_{\mathcal{C}}^{\max}$, giving rise to the generally nonlinear dynamics defined above. Although all maps contribute to the composition, the only inherently nonlinear map is $\mathcal{A}_{\mathcal{C}}^{\max}$ itself.

D. Complete positivity and trace preservation of the effective dynamics

In this section we prove that Γ_t is a nonlinear completely positive and trace-preserving (CPTP) map. To do this, we first show that both the assignment map and the effective dynamics are homogeneous of degree 1. This property implies trace preservation and will aid in the proof that both Γ_t and $\mathcal{A}_{\mathcal{C}}^{\max}$ are completely positive.

1. Homogeneity and trace preservation

As $\mathcal{C}$ and $\mathcal{V}_t$ are linear, and therefore homogeneous of degree 1, it suffices to prove the homogeneity of $\mathcal{A}_{\mathcal{C}}^{\max}$ to conclude that Γ_t is also homogeneous.

To proceed, consider an operator $\Delta = k\rho$, where $\rho \in \mathcal{S}(\mathsf{H}_d)$ is a density matrix and k is a real number. Thus, we have $k = \mathrm{tr}(\Delta)$. To extend the domain of $\mathcal{A}_{\mathcal{C}}^{\max}$ beyond density matrices and evaluate the assignment map on Δ, it suffices to incorporate k as the expectation value of the identity operator in Eq. (5), introducing its own Lagrange multiplier, that is, $k = \mathrm{tr}(\mathbb{1}_d \Delta) = \mathrm{tr}(\mathbb{1}_{d^n} \Delta_{\max}) = \mathrm{tr}(\Delta_{\max})$, where $\Delta_{\max}$ is the maximum entropy operator compatible with the normalization k and with any other expectation value constrained by Δ.

Since the identity operator commutes with all observables, it is easy to show that $\Delta_{\max} = k\varrho_{\max}$, where $\varrho_{\max}$ is the corresponding MaxEnt state compatible with Δ/k. Therefore, the extension of $\mathcal{A}_{\mathcal{C}}^{\max}$ to Hermitian operators is homogeneous of degree 1, that is,

$$\mathcal{A}_{\mathcal{C}}^{\max}(k\Delta) = k\mathcal{A}_{\mathcal{C}}^{\max}(\Delta)$$

for any real scalar k. Consequently, $\mathcal{A}_{\mathcal{C}}^{\max}$ is trace preserving on this space. This also implies, trivially, that Γ_t is trace preserving.

Provided that $\mathcal{A}_{\mathcal{C}}^{\max}$ and Γ_t map density matrices to density matrices, the homogeneity of $\mathcal{A}_{\mathcal{C}}^{\max}$ implies the positivity of both maps. Indeed, for any $\Delta \geqslant 0$ we have

$$\mathcal{A}_{\mathcal{C}}^{\max}(\Delta) = (\mathrm{tr}\Delta)\mathcal{A}_{\mathcal{C}}^{\max}\left(\frac{\Delta}{\mathrm{tr}\Delta}\right) \geqslant 0.$$

By construction, $\mathcal{A}_{\mathcal{C}}^{\max}(\Delta/\mathrm{tr}\Delta)$ is a density matrix [see Eq. (6)]. Since both $\mathcal{C}$ and $\mathcal{V}_t$ are positive maps, it follows that Γ_t is positive as well.

2. Complete positivity of the assignment map

To prove that Γ_t is completely positive, the crucial step is to show that $\mathcal{A}_{\mathcal{C}}^{\max}$ is completely positive. Due to the homogeneity of $\mathcal{A}_{\mathcal{C}}^{\max}$, it suffices to consider only density matrices in order to define its dilation. We denote this dilation by $\mathcal{A}_{\mathcal{C}\otimes\mathrm{id}_{\mathrm{E}}}^{\max}$ for any finite-dimensional ancillary system E. The dilation must satisfy the conditions

$$\begin{aligned} (\mathcal{C} \otimes \mathrm{id}_{\mathrm{E}}) \circ \mathcal{A}_{\mathcal{C}\otimes\mathrm{id}_{\mathrm{E}}}^{\max} &= \mathrm{id}_{\mathcal{S}(\mathsf{H}_d \otimes \mathsf{H}_{\mathrm{E}})}, \\ \mathcal{A}_{\mathcal{C}}^{\max}(\rho) &= \mathrm{tr}_{\mathrm{E}} \mathcal{A}_{\mathcal{C}\otimes\mathrm{id}_{\mathrm{E}}}^{\max}(\tilde{\rho}), \end{aligned} \tag{18}$$

with $\rho = \mathrm{tr}_{\mathrm{E}}\tilde{\rho}$. The first equation extends the consistency condition given in Eq. (16), while the second ensures that the effect of the dilation on the original system agrees with $\mathcal{A}_{\mathcal{C}}^{\max}(\rho)$.

To construct $\mathcal{A}_{\mathcal{C}\otimes\mathrm{id}_{\mathrm{E}}}^{\max}$, we apply the same procedure used to define $\mathcal{A}_{\mathcal{C}}^{\max}$, but now with $\mathcal{C} \otimes \mathrm{id}_{\mathrm{E}}$ as the coarse-graining map.

Consider a dilation of the microscopic description of the system with an ancillary system described by the Hilbert space H_E; since the extended coarse-graining map $\mathcal{C}\otimes \mathrm{id}_\mathrm{E}: \mathcal{B}(\mathsf{H}_d^{\otimes n}\otimes \mathsf{H}_\mathrm{E}) \to \mathcal{B}(\mathsf{H}_d\otimes \mathsf{H}_\mathrm{E})$ does not change the dimension of the extension, we will use H_E also for the dilation of the coarse-grained description. Thus, the total state of the extended microscopic system is $\tilde{\varrho}\in\mathcal{B}(\mathsf{H}_d^{\otimes n}\otimes\mathsf{H}_\mathrm{E})$. The next step is to extend the observables of the coarse-grained description

$$\varsigma^\alpha \mapsto \varsigma^\alpha\otimes \mathbb{1}_\mathrm{E}$$

such that $\langle\varsigma^\alpha\rangle = \mathrm{tr}((\varsigma^\alpha\otimes\mathbb{1}_\mathrm{E})\tilde{\rho}_\mathrm{eff})$, where $\tilde{\rho}_\mathrm{eff} = (\mathcal{C}\otimes\mathrm{id}_\mathrm{E})(\tilde{\varrho})$ is the effective extended state.

Since the assignment map consists of preparing the maximum entropy state compatible with the known expected values of ς_α, the following expression holds:

$$\mathrm{tr}((\varsigma^\alpha\otimes\mathbb{1}_\mathrm{E})\tilde{\rho}_\mathrm{eff}) = \mathrm{tr}((G^\alpha\otimes\mathbb{1}_\mathrm{E})\tilde{\varrho}_\mathrm{max}).$$

The G^α is defined in Eq. (4) and $\tilde{\varrho}_\mathrm{max}\in\mathcal{B}(\mathsf{H}_d\otimes\mathsf{H}_\mathrm{E})$ is the maximum entropy state compatible with the mean values defined above. To construct explicitly $\tilde{\varrho}_\mathrm{max}$ using the operators $G^\alpha\otimes\mathbb{1}_\mathrm{E}$, first observe that $\exp(G^\alpha\otimes\mathbb{1}_\mathrm{E}) = \exp(G^\alpha)\otimes\mathbb{1}_\mathrm{E}$; therefore, $\tilde{\varrho}_\mathrm{max} = \exp(\sum_{\alpha=1}^{d^2-1}\lambda_\alpha G^\alpha\otimes\mathbb{1}_\mathrm{E})/\tilde{Z} = \exp(\sum_{\alpha=1}^{d^2-1}\lambda_\alpha G^\alpha)\otimes\mathbb{1}_\mathrm{E}/\tilde{Z}$. Thus $\tilde{Z} = Z\times\dim\mathsf{H}_\mathrm{E}$ and the λ's coincide with the ones in Eq. (12). Therefore,

$$\begin{aligned}\mathcal{A}^{\max}_{\mathcal{C}\otimes\mathrm{id}_\mathrm{E}}(\tilde{\rho}_\mathrm{eff}) &:= \tilde{\varrho}_\mathrm{max} = \varrho_\mathrm{max}\otimes\frac{\mathbb{1}_\mathrm{E}}{\dim\mathsf{H}_\mathrm{E}}\\ &= \mathcal{A}^{\max}_{\mathcal{C}}(\rho_\mathrm{eff})\otimes\frac{\mathbb{1}_\mathrm{E}}{\dim\mathsf{H}_\mathrm{E}}\end{aligned} \tag{19}$$

holds, with $\rho_\mathrm{eff} = \mathrm{tr}_\mathrm{E}(\tilde{\rho}_\mathrm{eff})$. This result is expected considering that the given expectation values $\langle\varsigma^\alpha\rangle$ do not give any information about the ancillary system. At this point we have proven that $\tilde{\varrho}_\mathrm{max}$ is a density matrix for any finite-dimensional ancillary system E. Moreover, the homogeneity of $\mathcal{A}^{\max}_{\mathcal{C}\otimes\mathrm{id}_\mathrm{E}}$ on the space of Hermitian matrices implies complete positivity, i.e., $\mathcal{A}^{\max}_{\mathcal{C}\otimes\mathrm{id}_\mathrm{E}}(\tilde{\Delta})\geqslant 0$ for all $\tilde{\Delta}\geqslant 0$.

Observe that $\mathcal{A}^{\max}_{\mathcal{C}\otimes\mathrm{id}_\mathrm{E}}$ is not written in the usual fashion $\mathcal{A}^{\max}_{\mathcal{C}}\otimes\mathrm{id}_\mathrm{E}$ as it is nonlinear, but we were able to construct the extension anyway given that we can perform the preparation of the maximum entropy state compatible with the local observations, for any extension of the system. Moreover, notice that the formula in Eq. (19) trivially fulfills the conditions in Eq. (18).

3. *Complete positivity of* $\boldsymbol{\Gamma_t}$

The composition of linear CPTP maps is trivially CPTP due to the semigroup property of CPTP maps [11]. However, in our case, a nonlinear map is involved. To prove that Γ_t is CPTP, we compute its dilation based on the dilations of all constituent maps. The following scheme provides the details:

$$\begin{array}{ccc}\tilde{\rho}_\mathrm{eff}(0) & \xrightarrow{\ \tilde{\Gamma}_t\ } & \left(\rho_\mathrm{eff}(t)\otimes\frac{\mathbb{1}_\mathrm{E}}{\dim\mathsf{H}_\mathrm{E}}\right)\\ \Big\downarrow{\scriptstyle \mathcal{A}^{\max}_{\mathcal{C}\otimes\mathrm{id}_\mathrm{E}}} & & \Big\uparrow{\scriptstyle \mathcal{C}\otimes\mathrm{id}_\mathrm{E}}\\ \left(\varrho_\mathrm{max}(0)\otimes\frac{\mathbb{1}_\mathrm{E}}{\dim\mathsf{H}_\mathrm{E}}\right) & \xrightarrow{\ \gamma_t\otimes\mathrm{id}_\mathrm{E}\ } & \left(\varrho_\mathrm{max}(t)\otimes\frac{\mathbb{1}_\mathrm{E}}{\dim\mathsf{H}_\mathrm{E}}\right).\end{array}$$

Thus, the dilation of Γ_t results in

$$\begin{aligned}\tilde{\Gamma}_t &: \mathcal{S}(\mathsf{H}_d\otimes\mathsf{H}_\mathrm{E})\to\mathcal{S}(\mathsf{H}_d\otimes\mathsf{H}_\mathrm{E}),\\ &\tilde{\rho}_\mathrm{eff}(0)\mapsto \Gamma_t(\rho_\mathrm{eff}(0))\otimes\frac{\mathbb{1}_\mathrm{E}}{\dim\mathsf{H}_\mathrm{E}},\end{aligned} \tag{20}$$

where $\rho_\mathrm{eff}(0) = \mathrm{tr}_\mathrm{E}\tilde{\rho}_\mathrm{eff}(0)$. Therefore, $\tilde{\Gamma}_t(\tilde{\rho})$ is a density matrix for all $\tilde{\rho}\in\mathcal{B}(\mathsf{H}_d\otimes\mathsf{H}_\mathrm{E})$. This, combined with the homogeneity of the extension of $\tilde{\Gamma}_t$ to the space of Hermitian matrices (inherited from $\mathcal{A}^{\max}_{\mathcal{C}\otimes\mathrm{id}_\mathrm{E}}$), implies

$$\tilde{\Gamma}_t(\tilde{\Delta})\geqslant 0\,\forall\,\tilde{\Delta}\in\mathcal{B}(\mathsf{H}_d\otimes\mathsf{H}_\mathrm{E}),\quad \tilde{\Delta}\geqslant 0. \tag{21}$$

In conclusion, Γ_t is a nonlinear CPTP map.

III. EFFECTIVE NONLINEAR QUANTUM GATES

In light of the framework we have developed, and before examining the effective dynamics of n-qubit systems, we will focus our attention on simpler two-qubit systems, where the effect of the coarse-graining map on a microscopic state ϱ will be

$$\mathcal{C}(\varrho) = p_1\mathrm{tr}_2(\varrho) + p_2\mathrm{tr}_1(\varrho), \tag{22}$$

which is a convex combination of the reduced states of the two qubits and is equivalent to Eq. (2) for $n=2$. In particular, we will explore the effective dynamics generated by two well-known quantum gates: the SWAP gate and the controlled-NOT (CNOT) gate. We will see that the resulting effective dynamics is far from uninteresting. Indeed, the effective dynamics induced by these gates exhibit nonlinearity and non-Markovian behavior [39].

A. Effective SWAP gate

The Hamiltonian H_SWAP given by

$$H_\mathrm{SWAP} = \frac{\omega}{2}\sum_{\alpha\in\{x,y,z\}}\sigma^\alpha\otimes\sigma^\alpha \tag{23}$$

has the property of generating the SWAP gate for $t=\pi/2\omega$. Following the definition of Γ_t [Eq. (17)], we find that the effective state of the evolved system is given by

$$\begin{aligned}\mathcal{C}(U_\mathrm{SWAP}(t)\varrho_\mathrm{max}U^\dagger_\mathrm{SWAP}(t)) &= (p_1\sin^2\omega t + p_2\cos^2\omega t)\varrho_1\\ &\quad + (p_1\cos^2\omega t + p_2\sin^2\omega t)\varrho_2,\end{aligned}$$

where $U_\mathrm{SWAP}(t)$ is the unitary operator generated by the Hamiltonian (23). Since the effective initial state is given by Eq. (22), it is possible to see that the effective state's Bloch vector has a constant direction; only its length changes with time. This means that the effective dynamics corresponds to a depolarization channel where the depolarization coefficient depends on the initial state. To facilitate our analysis, let us define the Bloch vector's norm for the kth particle as $r_k = \tanh(p_k\lambda)$ and similarly denote the norm of the Bloch vector for the effective state by r_eff. With this, the quotient κ_t^eff between the norm of the Bloch vector of the initial effective state and the norm of the Bloch vector of the effective state at

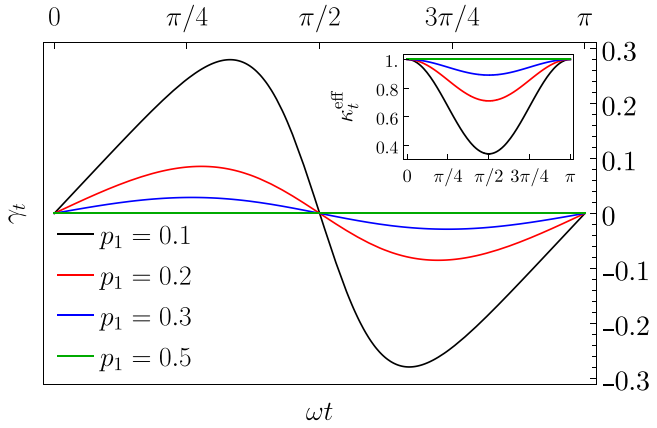

FIG. 1. Plot of the decay rate γ_t and the polarization coefficient κ_t^{eff} (inset) for different values of p_1, using an initial effective state with $r_{\text{eff}} = 0.9$. The decay rate exhibits both positive and negative values, indicating non-Markovian behavior in the dynamics.

time t is given by

$$\kappa_t^{\text{eff}} = \frac{1}{r_{\text{eff}}(0)}[p_1(r_1\cos^2\omega t + r_2\sin^2\omega t) + p_2(r_2\cos^2\omega t + r_1\sin^2\omega t)]. \tag{24}$$

This allows us to write the effective dynamics of the system as

$$\Gamma_t(\rho_{\text{eff}}) = \kappa_t^{\text{eff}}\rho_{\text{eff}} + \left(1-\kappa_t^{\text{eff}}\right)\tfrac{1}{2}\mathbb{1}. \tag{25}$$

Furthermore, since the effective dynamics is a depolarization channel, the evolution of the effective state is described by the Lindblad-like differential equation

$$\dot{\rho}_{\text{eff}} = \gamma_t \sum_{\alpha\in\{x,y,z\}} (\sigma^\alpha\rho_{\text{eff}}\sigma^\alpha - \rho_{\text{eff}}), \tag{26}$$

with $\gamma_t = -\dot{\kappa}_t^{\text{eff}}/4\kappa_t^{\text{eff}}$. A plot of the decay rate and the depolarization coefficient is shown in Fig. 1. This reveals that there are some scenarios where the effective state remains unchanged over time. For example, in the nonpreferential case where $p_1 = p_2$, the microscopic state is invariant under the SWAP gate [see Eq. (14)] and therefore the effective state remains invariant under the effective dynamics. In fact, it is easy to see that the depolarization coefficient (24) is equal to one when $p_1 = p_2$ (which is also shown in Fig. 1). Additionally, all pure states $|\phi\rangle\langle\phi|$ are also invariant under the effective dynamics, as long as no $p_k = 0$, since the only microscopic states compatible with such a macroscopic state is $|\phi\rangle\langle\phi|^{\otimes n}$, a symmetric state. Most interesting is that the decay rate γ_t is able to take negative values, indicating that, in addition to being nonlinear, the effective dynamics is non-Markovian [40–43]. Quantitatively, using the Breuer-Laine-Piilo measure in the interval shown in Fig. 1, we have [44]

$$\begin{aligned}\mathcal{M}_{\text{BLP}}[\Gamma_t] &= \int_{\dot{k}_t^{\text{eff}}>0} \dot{k}_t^{\text{eff}}dt \\ &= k_{\pi/\omega}^{\text{eff}} - k_{\pi/2\omega}^{\text{eff}} \\ &= \frac{(p_1-p_2)(r_1-r_2)}{r_{\text{eff}}(0)} \geqslant 0.\end{aligned} \tag{27}$$

The expression in the last line is always non-negative because $p_2 > p_1$ implies $r_2 > r_1$, and vice versa, since tanh is strictly increasing over the reals [see Eq. (11)].

To perform the optimization required to compute $\mathcal{M}_{\text{BLP}}$, we used the states $|0\rangle\langle 0|$ and $|1\rangle\langle 1|$; however, any pair of antipodal states on the Bloch sphere yields maximal distinguishability. This is because Γ_t is a nonlinear depolarizing channel that compresses or inflates the Bloch sphere in an isotropic manner.

B. Effective CNOT gate

Similarly to (23), the Hamiltonian

$$H_{\text{CNOT}} = -\frac{\omega}{2}(\sigma^z\otimes\mathbb{1} + \mathbb{1}\otimes\sigma^x - \sigma^z\otimes\sigma^x) \tag{28}$$

generates the CNOT gate at time $t = \frac{\pi}{2\omega}$. The effective dynamics at an arbitrary time t might be found by following the same procedure as in the previous case. However, the resulting expression is cumbersome and not very illuminating. Instead, we focus on the effective dynamics of the system at time $t = \frac{\pi}{2\omega}$, which is the time at which the CNOT gate is generated. The effective dynamics at this time is given by

$$\Gamma_{\text{CNOT}}(\rho_{\text{eff}}) = \tfrac{1}{2}\left[\rho_{\text{eff}} + p_1\mathcal{D}^z_{\langle\sigma_2^x\rangle}(\rho_1) + p_2\mathcal{D}^x_{\langle\sigma_1^z\rangle}(\rho_2)\right], \tag{29}$$

where $\mathcal{D}_q^\beta$ is a dephasing channel along the β direction with dephasing coefficient $1-q$. For example, if $\beta = z$, then

$$\mathcal{D}_q^z(\rho) = q\rho + (1-q)\sigma^z\rho\sigma^z; \tag{30}$$

that is, in (29) we encounter a convex combination of the effective state and two nonlinear state-dependent dephasing channels. Note that the usual interpretation of the CNOT gate is recovered, as we see that a bit flip (phase flip) is applied to the second (first) particle depending on the state of the first (second) particle. At an arbitrary time t, the effective dynamics is given by

$$\Gamma_t(\rho_{\text{eff}}) = \frac{1}{2}\rho_{\text{eff}} + \frac{p_1}{2}\mathcal{E}^x(\rho_{\text{eff}}) + \frac{p_2}{2}\mathcal{E}^z(\rho_{\text{eff}}), \tag{31}$$

where

$$\begin{aligned}\mathcal{E}^x(\rho_{\text{eff}}) = \rho_1\cos^2(\omega t) + \left[\langle\sigma_2^x\rangle\rho_1 + \left(1-\langle\sigma_2^x\rangle\right)\sigma^z\rho_1\sigma^z\right] \\ \times\sin^2(\omega t) - i\left(1-\langle\sigma_2^x\rangle\right)\cos(\omega t)\sin(\omega t)[\rho_1,\sigma^z]\end{aligned}$$

and

$$\begin{aligned}\mathcal{E}^z(\rho_{\text{eff}}) = \rho_2\cos^2(\omega t) + \left[\langle\sigma_1^z\rangle\rho_2 + \left(1-\langle\sigma_1^z\rangle\right)\sigma^x\rho_2\sigma^x\right] \\ \times\sin^2(\omega t) - i\left(1-\langle\sigma_1^z\rangle\right)\cos(\omega t)\sin(\omega t)[\rho_2,\sigma^x].\end{aligned}$$

In Appendix B we show that $\mathcal{E}^z$ and $\mathcal{E}^x$ are channels that describe elliptical trajectories on the Bloch sphere. This is because they correspond to the reduced dynamics of two two-level systems that evolve according to a nonlocal Hamiltonian [45].

IV. EFFECTIVE SPIN CHAIN DYNAMICS

Now that we have seen that nonlinear, non-Markovian results arise from the coarse-grained dynamics of a two-qubit system, we study larger many-body systems, such as the spin chains.

A. Nonuniform external magnetic field with all-to-all interactions

First, we consider spin-1/2 chains evolving in a nonuniform external magnetic field in the z direction with an all-to-all Ising interaction parallel to the field. The Hamiltonian considered is thus

$$H = H_{\text{field}} + H_{\text{int}}, \tag{32}$$

where

$$H_{\text{field}} = \sum_k \omega_k \sigma_k^z, \quad H_{\text{int}} = (\sigma^z)^{\otimes n}. \tag{33}$$

Since the field and interaction terms commute, it is possible to solve them separately.

Let us first consider the magnetic-field part of the Hamiltonian, which leads to an effective evolution that is a combination of all the local evolutions. Indeed, because all terms in H_{field} commute, the corresponding unitary evolution is

$$U_{\text{field}}(t) = \prod_k U_k(t), \tag{34}$$

where $U_k(t) = e^{-i\omega_k t \sigma_k^z}$. Applying the coarse-graining map to the maximum entropy stated evolved through (34) yields

$$\Gamma_t^{\text{field}}(\rho_{\text{eff}}) = \sum_k p_k U_k(t) \rho_k U_k^\dagger(t), \tag{35}$$

where ρ_k are the subsystems defined by the maximum entropy assignment map (9).

We now show that in scenarios where a dominant probability prevails, the state evolution described by Eq. (35) tends to spiral down towards a unitary evolution into a more mixed state. Specifically, each term in the summation of Eq. (35) circles the z axis. However, given random frequencies, these movements are incoherent. This lack of coherence manifests completely after a specific time, defined as $t_c = 2\pi/\varsigma$, where ς represents the standard deviation of the frequencies ω_k. At this juncture, under appropriate conditions, the phases $\exp(i\omega_k t)$ distribute uniformly around the whole unit circle. In scenarios where one probability, such as p_1, significantly surpasses others and there is a large number of particles, the dominant effect is a singular weakened contribution

$$\lim_{\substack{n\to\infty \\ t>t_c}} \Gamma_t^{\text{field}}(\rho_{\text{eff}}) \to U_1(t) \mathcal{P}_{p_1 r_1}(\rho_{\text{eff}}) U_1^\dagger(t), \tag{36}$$

where $\mathcal{P}_q(\rho) = q\rho + (1-q)\mathbb{1}/d$ is a depolarizing channel. Thus, after t_c, the dynamics converges to a limit cycle in the Bloch sphere representation [see Fig. 2(a)]. In fact, the fluctuations around this evolution will decrease as approximately $1/\sqrt{n}$, since we would be effectively adding $n-1$ random numbers on top of the preferred evolution [see Fig. 2(b)]. This convergence reflects how dominant probabilities influence the system's evolution, simplifying the overall dynamics to primarily one major contribution. The contraction of the resulting state with respect to the initial one is a consequence of the loss of information about the nonpreferential particles. This loss of information arises due to the averaging process of the preferential measurement, which effectively discards information about the other particles and makes the effective state more mixed. It is worth adding that if there is no preferential particle, we will observe the qubit simply spiraling towards the origin in the x-y plane while keeping the z component constant.

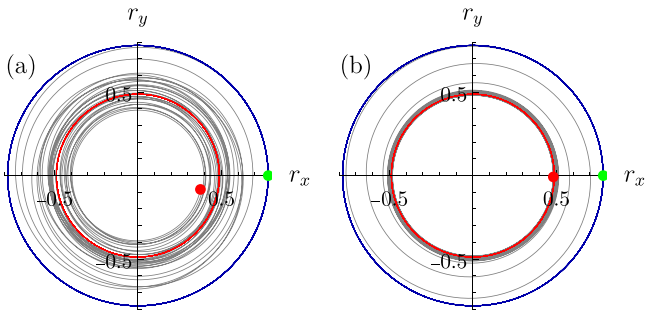

FIG. 2. Effective evolution of the macroscopic state's Bloch vector for (a) $n = 10$ and (b) $n = 500$ particles under the Hamiltonian H_{field} with frequencies ω_k normally distributed with mean $\mu = 1.5$ and standard deviation $\varsigma = 0.2$ (manifested in the variation of the gray curve around the limit cycle). The green point represents the state at $t = 0$ and the red point denotes the state at the final time $t = 4t_c$. The effective state oscillates around a mean evolution (red) of radius $p_1 r_1$, with $p_1 = 0.5$. Comparing the two plots, its possible to appreciate the decrease of the fluctuations, which is proportional to $1/\sqrt{n}$.

Having solved the free part of the Hamiltonian, we now focus on the interaction term. It can be shown, either by applying the coarse-graining map to the evolved microscopic state or by applying it to the Liouville–von Neumann equation, that the interaction part of the Hamiltonian leads approximately to a nonunitary but linear evolution. Consider the Liouville–von Neumann equation

$$\dot{\varrho}_{\max} = -i[(\sigma^z)^{\otimes n}, \varrho_{\max}] \tag{37}$$

and solve it by iteratively integrating and substituting the implicit solution in the commutator, from which we obtain the power series in H_{int}. Applying the coarse-graining map and taking into account its linearity, we arrive at

$$\Gamma_t^{\text{int}}(\rho_{\text{eff}}) = \rho_{\text{eff}}(0) + (-it)\mathcal{C}([H_{\text{int}}, \varrho_{\max}(0)]) + \frac{(-it)^2}{2!}\mathcal{C}([H_{\text{int}}, [H_{\text{int}}, \varrho_{\max}(0)]]) + \cdots. \tag{38}$$

To work with Eq. (38), we notice that the nested commutators can be expressed as

$$[[b]H_{\text{int}}, \underbrace{\ldots, [H_{\text{int}},}_{n \text{ times}} \varrho_{\max}(0)]] = \begin{cases} 2^{n-1}[H_{\text{int}}, \varrho_{\max}(0)], & \text{odd } n \\ 2^{n-1}[\varrho_{\max}(0) - H_{\text{int}}\varrho_{\max}(0)H_{\text{int}}], & \text{even } n. \end{cases} \tag{39}$$

Using this, we can integrate the von Neumann equation as usual to obtain two different power series, corresponding to even and odd powers of t. Then we can neglect the terms with odd powers of t in the limit of large N, because $\mathcal{C}\{[H_{\text{int}}, \varrho_{\max}(0)]\}$ decreases exponentially with the number of particles. This will lead us to find that the effective evolution for big N is

$$\Gamma_t^{\text{int}}(\rho_{\text{eff}}) = \mathcal{D}^z_{\cos^2(t)}(\rho_{\text{eff}}), \tag{40}$$

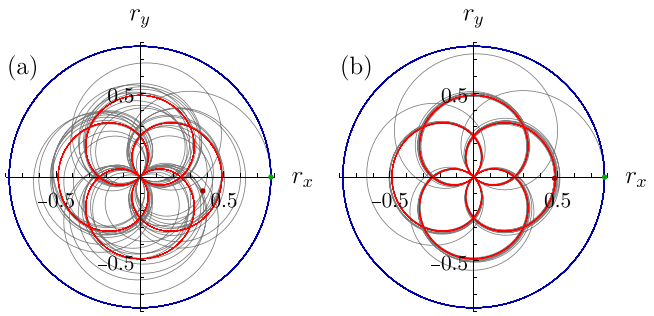

FIG. 3. Plot of the effective evolution of a set of particles, under the Hamiltonian (32) for (a) $n = 10$ and (b) $n = 500$ particles. See the caption of Fig. 2 for the color coding. The frequencies are chosen in an identical manner, as well as the probability distribution and the evolution time. In this case, the asymptotic evolution, in red, corresponds to Eq. (41).

i.e., a dephasing channel in the z direction with oscillating intensity. For details regarding the calculation stated in this paragraph, see Appendix D.

Now that we have found the solutions to both the local and interaction parts of the Hamiltonian to be given by (35) and (40), respectively, and given that both dynamics commute, we can say that the effective evolution will be the composition of these two, that is,

$$\lim_{\substack{n\to\infty \\ t>t_c}} \Gamma_t(\rho_{\text{eff}}) \to \mathcal{D}^z_{\cos^2(t)}\big(U_1(t)\mathcal{P}_{p_1 r_1}(\rho_{\text{eff}})U_1^\dagger(t)\big). \tag{41}$$

For times much larger than t_c, the effective state's Bloch vector will oscillate around the composition of the evolution of the preferred subsystem and the dephasing channel, i.e., a polar rose, as shown in Fig. 3. In cylindrical coordinates, we can write

$$r(t) = r(0)\cos[\theta(t)], \tag{42}$$

$$\theta(t) = \frac{t}{\omega_1} + \theta(0), \tag{43}$$

$$z(t) = z(0). \tag{44}$$

It is important to underline that such dynamics is obtained assuming a large number of particles. This allows us to write the interaction part of the evolution as a dephasing channel, i.e., as a straight line. For finite n, a squeezed elliptical trajectory is found. Moreover, the actual trajectory will oscillate around Eq. (41) with an amplitude proportional to $1/\sqrt{n}$.

So far, our discussion of the dynamics induced by Hamiltonian (32) has centered around the use of the preferential distribution (3). For the nonpreferential case, the situation is analogous. Indeed, without interaction, the dynamics will once again follow (36). However, since the depolarization of the state will have a coefficient r_{eff}/n, it will effectively converge to a point on the z axis. On the other hand, for the interacting case, the state's trajectory will follow the shape of the appropriate rose, but with an increasingly small amplitude, until it also collapses to the z axis.

B. Ising chain

We now consider a homogeneous and closed Ising spin-1/2 chain coupled to a transversal magnetic field. The governing Hamiltonian is

$$H = -J\sum_{j=1}^{N}\sigma_j^z\sigma_{j+1}^z - g\sum_{j=1}^{N}\sigma_j^x, \quad \sigma_{N+1}^z \equiv \sigma_1^z. \tag{45}$$

This Hamiltonian is invariant under spin translations, that is, changing indices $j \to j+1$. We study the case when the effective initial state is pure,

$$|\psi\rangle = \cos\left(\frac{\theta}{2}\right)|0\rangle + ie^{i\phi}\sin\left(\frac{\theta}{2}\right)|1\rangle.$$

When all particles participate in the coarse graining, i.e., they have nonzero probabilities in Eq. (2), the only compatible microscopic state is $|\psi\rangle^{\otimes N}$, given that pure states are extremal.

Moreover, observe that the reduced dynamics of one spin is the same for every spin due to the translation symmetry of the Hamiltonian and the permutation symmetry of the initial state. If we denote the reduced density matrix of the kth particle at a time t by $\rho_k(t)$, this implies that $\rho_k(t) = \rho_l(t)$ for every t, k, and l. Consequently, the effective state at time t is simply $\rho_{\text{eff}}(t) = \rho_k(t)$ for any k. Therefore, the effective dynamics and the microscopic state are independent of the exact values of p_k, provided all of them are nonzero ($p_k > 0\,\forall\, k$).

Let us now discuss the results. For $g/J = 0$ the system is tractable analytically (see Appendix C for details). For this case, the reduced dynamics is a nonlinear dephasing with rotation around the z axis,

$$\rho_{\text{eff}}(t) = \begin{pmatrix} \cos^2\left(\frac{\theta}{2}\right) & \gamma(\theta,t)\frac{1}{2}e^{-i\phi}\sin(\theta) \\ \gamma^*(\theta,t)\frac{1}{2}e^{i\phi}\sin(\theta) & \sin^2\left(\frac{\theta}{2}\right) \end{pmatrix}, \tag{46}$$

with

$$\gamma(\theta,t) = [\cos(2Jt) + i\cos(\theta)\sin(2Jt)]^2. \tag{47}$$

The dynamics is nonlinear and does not depend on the total number of spins in the chain. Moreover, it depends only on θ (see Fig. 4); this is expected due to the azimuthal symmetry of the Hamiltonian. Furthermore, both dephasing and rotation depend on θ; therefore, there is a differential rotation apart from the nonlinear dephasing, depicted by the twisted white wires in the figures.

For $g/J > 0$, we performed numerical calculations without approximations for 2252 initial pure states, uniformly distributed to resemble the polygon mesh representation of the Bloch sphere. In Fig. 4 we present the results for $N = 8$, where it can be observed that the dynamics becomes increasingly intricate as g/J increases.

In our numerical experiments, we observed that the results are visually indistinguishable for $N \geqslant 4$. Since increasing the system's size is computationally expensive, we analyzed how uniformly random effective initial states vary with respect to the finer system's size. To do this, we evolved each random state over multiple time points, particle numbers at the finer level, and different several values of g/J.

For comparison, in Fig. 5 we plot the trace distance between states evolved with consecutive particle numbers, while

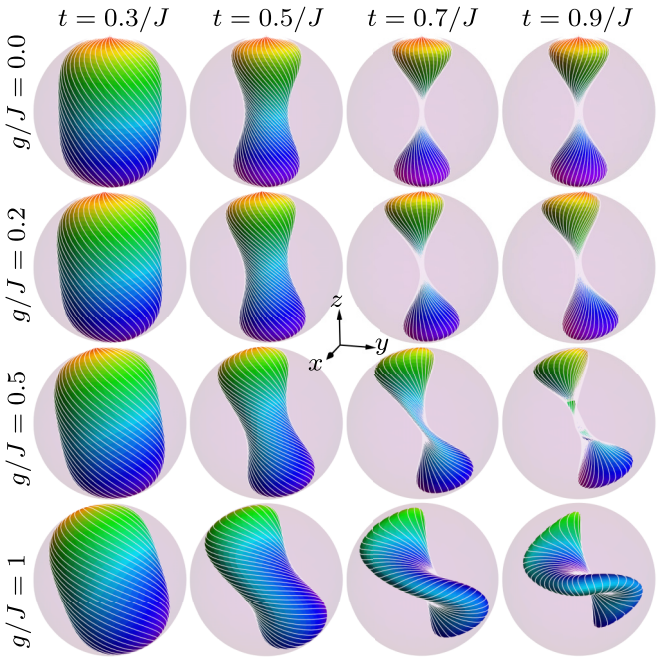

FIG. 4. Evolution of the Bloch sphere containing all initial pure states for several values of field coupling and time, with eight qubits in the fine transverse-field Ising dynamics. The color code is as follows: A gradient from north (red) to south (blue) represents different polar angles, while white wires indicate families of states with a fixed azimuthal angle. The effective dynamics is nonlinear in all cases; in particular, for $g/J = 0$, it corresponds to nonlinear dephasing with differential rotation around the z axis (illustrated by the twisted white wires). See the text for further details.

the inset shows the trace distance with respect to the case of eight particles (recalling that Fig. 4 was produced with eight particles). As g/J increases, the error grows slightly but still decays rapidly. With respect to the system with eight particles (inset in Fig. 5), the error becomes negligible, indicating that

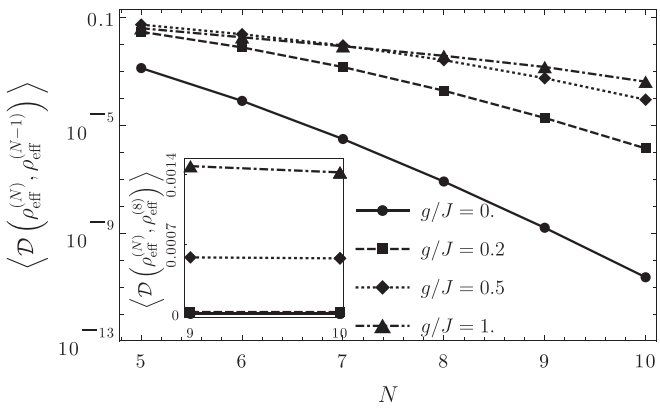

FIG. 5. Average trace distance of effective states evolved with different numbers of particles at a finer level. The main plot shows the average trace distance between consecutive particle numbers. The inset displays the average trace distance for nine and ten particles with respect to the case of eight particles. The average is taken over multiple time points and 100 quantum states.

the results shown in Fig. 4 are close to those of the thermodynamic limit ($N \to \infty$).

V. LINEAR EFFECTIVE DYNAMICS

In Sec. III we presented two examples of microscopic dynamics that give rise to a nonlinear, non-Markovian evolution of the effective state. Nevertheless, not all microscopic dynamics will produce such behavior of the effective dynamics. In this section we present some examples of evolution for which the linearity is preserved under the coarse-graining map.

A. Channels that act equally on all subsystems

First, let $\mathcal{E}$ be a quantum channel acting on a two-level system

$$\mathcal{E} : \mathcal{B}(\mathsf{H}_2) \to \mathcal{B}(\mathsf{H}_2) \tag{48}$$

and let ϱ be the density operator that describes a collection of n such units. We define $\mathcal{E}^{\otimes n}$ as $\mathcal{E}$ applied locally to each of the subsystems of the n-partite system,

$$\mathcal{E}^{\otimes n} : \mathcal{B}\big(\mathsf{H}_2^{\otimes n}\big) \to \mathcal{B}\big(\mathsf{H}_2^{\otimes n}\big), \tag{49}$$

according to

$$(\mathcal{E} \otimes \mathcal{E})(A \otimes B) = \mathcal{E}(A) \otimes \mathcal{E}(B) \tag{50}$$

for any $A, B \in \mathcal{B}(\mathsf{H}_2)$. By expanding ϱ in the basis of tensor products of the Pauli matrices, it is a matter of algebra to show that

$$(\mathcal{C} \circ \mathcal{E}^{\otimes n})(\varrho) = (\mathcal{E} \circ \mathcal{C})(\varrho) \tag{51}$$

for any $\varrho \in \mathcal{S}(\mathsf{H}_2^{\otimes n})$. This means that all channels that act locally and in the same way over all subsystems conserve their linearity under the coarse-graining map. Furthermore, nonfactorizable channels that act equally upon all reduced matrices also conserve their linearity.

As a first example, let us consider dephasing channel. An n-qubit total dephasing channel in the z direction is

$$\mathcal{D}^z_{1/2^n}(\varrho) = \frac{1}{2^n} \sum_{\vec{\alpha}} (\sigma^{\vec{\alpha}}) \varrho (\sigma^{\vec{\alpha}})^\dagger, \tag{52}$$

where $\sigma^{\vec{\alpha}} = \sigma^{\alpha_1} \otimes \cdots \otimes \sigma^{\alpha_n}$ with $\alpha_j \in \{0, z\}$. It is not difficult to see that

$$\mathcal{C}\big(\mathcal{D}^z_{1/2^n}(\varrho)\big) = \mathcal{D}^z_{1/2}(\mathcal{C}(\varrho)), \tag{53}$$

that is, the total dephasing channel on the microscopic system translates under the coarse-graining map as a total dephasing channel over the effective system. The total dephasing channel is an example of a factorizable Pauli component erasing map [46]. A nonfactorizable Pauli component erasing map that is also a quantum channel is

$$\mathcal{E} : \mathcal{B}\big(\mathsf{H}_2^2\big) \to \mathcal{B}\big(\mathsf{H}_2^2\big), \quad \varrho = \frac{1}{4} \sum_{\vec{\alpha}} \gamma_{\vec{\alpha}} \sigma^{\vec{\alpha}} \to \frac{1}{4} \sum_{\vec{\alpha}} \gamma_{\vec{\alpha}} \tau_{\vec{\alpha}} \sigma^{\vec{\alpha}}, \tag{54}$$

with

$$\begin{pmatrix} \tau_{0,0} & \tau_{0,x} & \tau_{0,y} & \tau_{0,z} \\ \tau_{x,0} & \tau_{x,x} & \tau_{x,y} & \tau_{x,z} \\ \tau_{y,0} & \tau_{y,x} & \tau_{y,y} & \tau_{y,z} \\ \tau_{z,0} & \tau_{z,x} & \tau_{z,y} & \tau_{z,z} \end{pmatrix} = \begin{pmatrix} 1 & 0 & 1 & 0 \\ 0 & 1 & 0 & 1 \\ 1 & 0 & 1 & 0 \\ 0 & 1 & 0 & 1 \end{pmatrix}. \tag{55}$$

Note that this $\mathcal{E}$ acts equally on both reduced density matrices. In fact, it acts as a dephasing channel in the y direction upon both subsystems, and so

$$\mathcal{C}(\mathcal{E}(\varrho)) = \mathcal{D}^{y}_{1/2}(\mathcal{C}(\varrho)). \tag{56}$$

Although this is an example for two two-level systems, all n-qubit quantum channels that satisfy

$$\mathrm{tr}_{\bar{j}}(\mathcal{E}(\varrho)) = \mathrm{tr}_{\bar{k}}(\mathcal{E}(\varrho))\,\forall\, k, j \in \{1, \ldots, n\} \tag{57}$$

will give rise to linear effective dynamics.

B. Linear non-Markovian evolution

Another instance of a microscopic evolution that preserves its linearity under the coarse-graining map is the given by the Hamiltonian

$$H = \frac{\omega}{2}(\mathbb{1} \otimes \sigma^{z}). \tag{58}$$

Clearly, this is not a mapping that abides by the condition stated by Eq. (57). However, as we will see, the effective dynamics remain linear with a notable twist: They are non-Markovian. Indeed, using the nonpreferential distribution described in Eq. (3), the microscopic evolution (58) induces the macroscopic dynamics given by

$$\Gamma_t(\rho_{\mathrm{eff}}) = \tfrac{1}{2}\left(\rho_{\mathrm{eff}} + e^{-i(\omega t/2)\sigma^{z}}\rho_{\mathrm{eff}}e^{i(\omega t/2)\sigma^{z}}\right), \tag{59}$$

and its effect on the evolution of the effective Bloch vector is described by the parametric equations

$$r^{x}_{\mathrm{eff}}(t) = \tfrac{1}{2}\left[r^{x}_{\mathrm{eff}}\cos(\omega t) - r^{y}_{\mathrm{eff}}\sin(\omega t) + r^{x}_{\mathrm{eff}}\right], \tag{60}$$

$$r^{y}_{\mathrm{eff}}(t) = \tfrac{1}{2}\left[r^{y}_{\mathrm{eff}}\cos(\omega t) + r^{x}_{\mathrm{eff}}\sin(\omega t) + r^{y}_{\mathrm{eff}}\right], \tag{61}$$

$$r^{z}_{\mathrm{eff}}(t) = r^{z}_{\mathrm{eff}}, \tag{62}$$

which represent the parametric equations of a circle in $\mathbb{R}^3$ with center at $(r^{x}_{\mathrm{eff}}/2, r^{y}_{\mathrm{eff}}/2, r^{z}_{\mathrm{eff}})$, parallel to the x-y plane, and with radius $\frac{1}{2}\sqrt{(r^{x}_{\mathrm{eff}})^2 + (r^{y}_{\mathrm{eff}})^2}$.

The differential equation governing the effective dynamics is

$$\frac{\mathrm{d}\rho}{\mathrm{d}t} = -i\left[\frac{\omega}{4}\sigma^{z}, \rho\right] + \frac{\omega}{2}\tan\left(\frac{\omega t}{2}\right)(\sigma^{z}\rho\sigma^{z} - \rho). \tag{63}$$

From this differential equation, we can identify the effective Hamiltonian as

$$H_{\mathrm{eff}} = \frac{\omega}{4}\sigma^{z}, \tag{64}$$

where the frequency appearing in the effective Hamiltonian is reduced by half compared to the frequency of the microscopic Hamiltonian. It is worth noting that Eq. (63) exhibits singularities at points where the tangent function diverges.

Since the term $\tan(\frac{\omega t}{2})$ can be positive or negative, the dynamics is generally non-Markovian. Furthermore, it is straightforward to verify that the corresponding dynamics in (59) do not satisfy the semigroup property:

$$\Gamma_{t+s}(\rho) \neq \Gamma_t(\Gamma_s(\rho)). \tag{65}$$

Thus, coarse-grained quantum dynamics adds to the wide variety of physical systems that exhibit non-Markovianity [47].

VI. CONCLUSION

We introduced a pragmatic notion of effective dynamics for coarse-grained descriptions of conventional many-body quantum systems. To achieve this, we used the maximum entropy principle to deal with the fact that the effective description emerges from a coarse-graining map that irreversibly destroys part of the microscopic information. This method is quite appealing given that no additional information or assumptions are introduced to construct the microscopic state of the system. We assumed that the latter undergoes unitary evolution and thus the system is closed. Remarkably, the emergent dynamics is generally nonlinear and depends on both the initial effective state and the probability distribution that defines the coarse-graining map.

Additionally, we have proven that such dynamics defines nonlinear completely positive and trace-preserving maps. We believe that this is a beneficial trait given that complete positivity implies positivity, and classical stochastic maps are positive [40]. Moreover, in the absence of quantum correlations, complete positivity is reduced to positivity [48]. This ensures consistency if we consider this framework to investigate the quantum-to-classical transition.

We studied several systems to test the framework, ranging from quantum gates to spin systems. They show explicitly the dependence on the distribution of the coarse-graining map and on the initial effective states. However, in the case of the Ising spin chain, its symmetries conceal the effective dynamics from the exact values of the distribution, except that they must be greater than zero. It is worth noting that effective dynamics is not always nonlinear, as shown in Sec. V B. Interestingly, this example is nonlinear and non-Markovian; thus, closed (and trivially Markovian) microscopic dynamics leads to non-Markovianity.

The proposed framework has both fundamental and practical applications. On the fundamental side, it contributes to understanding how effective nonlinearity can emerge from the combination of linear Schrödinger dynamics and addressing errors. This perspective may offer insights into the quantum-to-classical transition at the level of dynamical evolution. However, further investigations are needed to explore this connection in greater depth. On the practical side, when analyzing the dynamics of quantum many-body systems, such as spin lattices [49] or IBM quantum processors with various hardware geometries [50], the framework provides a principled basis for identifying and quantifying a source of decoherence. Notably, in systems with many particles, the cumulative effect of addressing errors can become significant even when individual error probabilities remain small, due to the exponential sensitivity [20].

Finally, several questions arise from this work. For example, under what conditions does the emergent nonlinearity depend only on the distribution of the coarse graining?

Inspired by the Ising spin chain, is it possible to find nonlinear dynamics that is independent of the initial state?

ACKNOWLEDGMENTS

It is with great pleasure that we thank Fernando de Melo, Raul Vallejo, and Hamed Mohammady for their useful comments and suggestions. We acknowledge project VEGA No. 2/0183/21 (DESCOM). This work was supported by UNAM-PAPIIT Grant No. IG101324.

DATA AVAILABILITY

The data that support the findings of this article are openly available [51].

APPENDIX A: FUZZY OPERATORS

In this Appendix we show the relation between the expected values of a tomographically complete set of observables on the effective Hilbert space $\{\varsigma^\alpha\}_\alpha$ and the expected values of what we call fuzzy operators. Recalling that the effective and the microscopic states are related through $\rho_{\text{eff}} = \mathcal{C}(\varrho)$, we can write

$$\begin{aligned}
\text{tr}(\varsigma^\alpha \rho_{\text{eff}}) &= \text{tr}[\varsigma^\alpha \mathcal{C}(\varrho)] \\
&= \text{tr}\left[\varsigma^\alpha \text{tr}_{\bar{1}}\left(\sum_{k=1}^{n} p_k P_{1,k}\varrho P_{1,k}\right)\right] \\
&= \text{tr}\left(\varsigma_1^\alpha \sum_{k=1}^{n} p_k P_{1,k}\varrho P_{1,k}\right) && \text{(A1)} \\
&= \sum_{k=1}^{n} p_k \text{tr}\left(\varsigma_1^\alpha P_{1,k}\varrho P_{1,k}\right) && \text{(A2)} \\
&= \sum_{k=1}^{n} p_k \text{tr}\left(P_{1,k}\varsigma_1^\alpha P_{1,k}\varrho\right) && \text{(A3)} \\
&= \text{tr}\left[\left(\sum_{k=1}^{n} p_k P_{1,k}\varsigma_1^\alpha P_{1,k}\right)\varrho\right] && \text{(A4)} \\
&= \text{tr}\left[\left(\sum_{k=1}^{n} p_k \varsigma_k^\alpha\right)\varrho\right], && \text{(A5)}
\end{aligned}$$

where we have used the fact that swaps $P_{j,k}$ are Hermitian and the cyclic property of the trace. Additionally, ς_k^α is the observable ς^α applied to the kth particle. Finally, we can identify the operators G^α as defined in (4) where the following holds:

$$\text{tr}(\varsigma^\alpha \rho_{\text{eff}}) = \text{tr}(G^\alpha \varrho). \tag{A6}$$

APPENDIX B: ELLIPTIC CNOT PATH

Here we show that the interaction term of the CNOT Hamiltonian, $\sigma^z\sigma^x$, results in an elliptical path for the Bloch vector of the effective state. First, it is easy to show [45] that if we assume that the initial microscopic state is a product state, then the reduced Bloch vectors evolve according to

$$\begin{aligned}
r_1^x(t) &= r_1^x(0)\cos(t) + r_1^y(0) r_2^x(0)\sin(t), \\
r_1^y(t) &= r_1^y(0)\cos(t) - r_1^x(0) r_2^x(0)\sin(t), \\
r_1^z(t) &= r_1^z(0)
\end{aligned} \tag{B1}$$

and

$$\begin{aligned}
r_2^x(t) &= r_2^x(0), \\
r_2^y(t) &= r_2^y(0)\cos(t) - r_1^z(0) r_2^z(0)\sin(t), \\
r_2^z(t) &= r_2^z(0)\cos(t) + r_1^z(0) r_2^y(0)\sin(t),
\end{aligned} \tag{B2}$$

which correspond to ellipses confined to the x-y and y-z planes. The Bloch vector of the effective state is of course the sum of the Bloch vectors of the two qubits, and thus the effective Bloch vector evolves according to

$$\vec{r}_{\text{eff}} = p_1\vec{r}_1 + p_2\vec{r}_2. \tag{B3}$$

As it turns out, this is also an ellipse, as it can be written as

$$\vec{r}_{\text{eff}} = \vec{u}\sin(t) + \vec{v}\cos(t) + \vec{c}. \tag{B4}$$

Here

$$\vec{u} = \begin{bmatrix} -b_1 p_1 \sin(\theta_1) \\ p_1[a_1\sin(\theta_1) + b_1\cos(\theta_1)] \\ p_2[a_2\sin(\theta_2) + b_2\cos(\theta_2)] \end{bmatrix}, \tag{B5}$$

$\vec{c} = [p_2 x_2(0) \quad 0 \quad p_1 z_1(0)]^T$, and

$$\vec{v} = \begin{bmatrix} a_1 p_1 \cos(\theta_1) \\ p_2[a_2\cos(\theta_2) - b_2\sin(\theta_2)] \\ 0 \end{bmatrix}. \tag{B6}$$

The parameters a_j, b_j, and θ_j correspond to the ellipse parameters of the path followed by each reduced system and are related to their initial Bloch vectors through

$$\begin{aligned}
a_1\cos(\theta_1) &= r_1^x(0), \quad a_1\sin(\theta_1) = -r_1^y(0), \\
b_1\cos(\theta_1) &= -r_1^x(0) r_2^x(0), \quad b_1\sin(\theta_1) = r_1^y(0) r_2^x(0)
\end{aligned}$$

and

$$\begin{aligned}
a_2\cos(\theta_2) &= r_2^y(0), \quad a_2\sin(\theta_2) = -r_2^z(0), \\
b_2\cos(\theta_2) &= r_1^z(0) r_2^y(0), \quad b_2\sin(\theta_2) = -r_1^z(0) r_2^z(0).
\end{aligned}$$

APPENDIX C: ISING MODEL WITHOUT MAGNETIC FIELD

As mentioned in the main text, to compute the coarse-grained state of the spin chain after the unitary evolution of the microscopic description with $g/J = 0$, it is enough to compute the reduced density matrix for any spin. To do it, first observe that due to the translation symmetry and the specific form of the initial state $|\psi\rangle^{\otimes N}$, the reduced evolution for each spin is identical. The density matrix of the initial pure state of the spin tagged with $N-1$, $|\psi\rangle = \cos(\theta/2)|0\rangle + e^{i\phi}\sin(\theta/2)|1\rangle$, in the computational basis is

$$\rho_{N-1}(0) = \begin{pmatrix} \cos^2\left(\frac{\theta}{2}\right) & \frac{1}{2}e^{-i\phi}\sin(\theta) \\ \frac{1}{2}e^{i\phi}\sin(\theta) & \sin^2\left(\frac{\theta}{2}\right) \end{pmatrix},$$

and the total density matrix of the microscopic description, also in the computational basis, is

$$(|\psi\rangle\langle\psi|)^{\otimes N} = \sum_{\vec{k},\vec{l}} C_k^N C_l^N e^{i(\phi+\pi/2)(l-k)} c_\theta^{k+l} s_\theta^{2N-k-l} |\vec{k}\rangle\langle\vec{l}|, \tag{C1}$$

with C_k^N and C_l^N the binomial coefficients where k and l are the numbers of 0's in $\vec{k}$ and $\vec{l}$, respectively. We also use the abbreviations $c_\theta := \cos(\theta/2)$ and $s_\theta := \sin(\theta/2)$. To derive its evolution it is enough to compute the components $[\rho_{N-1}(t)]_{00}$ and $[\rho_{N-1}(t)]_{01}$. Now observe the following: When tracing out all spins except $N-1$, only operators with the form $|0\vec{i}\rangle\langle 0\vec{i}|$ contribute to $|0\rangle\langle 0|$, where $\vec{i}$ is a vector indicating the rest of the 0's and 1's of the computational basis. Since $|0\vec{i}\rangle$ is an eigenstate of the Hamiltonian, the component $[\rho_{N-1}(t)]_{00} = [\rho_{N-1}(0)]_{00}$ remains invariant.

For $[\rho_{N-1}(t)]_{01}$ only operators with the form $|0\vec{i}\rangle\langle 1\vec{i}|$ contribute to the partial trace. Thus, let us investigate their evolution. Observe that both $|0\vec{i}\rangle$ and $|1\vec{i}\rangle$ are eigenvectors of the evolution operator of the spin chain. Therefore, assume that

$$U(t)|0\vec{i}\rangle = e^{itE_{0\vec{i}}}|0\vec{i}\rangle,$$

where $E_{0\vec{i}}$ is the eigenenergy of $|0\vec{i}\rangle$. Now we want to find the relative phase with $|1\vec{i}\rangle$. To do this it is enough to observe what happens with the nearest neighbors of $N-1$ (spins 0 and $N-2$). So we need to investigate the changes in just four configurations: 0**0**0. Starting with 000, where the spin at the center is $N-1$ and others are its neighbors, changing it to 010 "removes" two $+J$ terms in the eigenenergy expression of state $|00\vec{i}'0\rangle$ in favor of two $-J$ terms; thus

$$U(t)|10\vec{i}'0\rangle = e^{it(E_{0\vec{i}}-4J)}|10\vec{i}'0\rangle,$$

where the leftmost spin is the one tagged with $N-1$ and the other spins indicated explicitly are its neighbors. The vector $\vec{i}'$ contains the rest of the spins in the computational basis. Putting both kets together we have

$$U(t)|00\vec{i}'0\rangle\langle 10\vec{i}'0|U(-t) = e^{it4J}|00\vec{i}'0\rangle\langle 10\vec{i}'0|.$$

To compute how operators $|00\vec{i}'\rangle\langle 10\vec{i}'0|$ contribute to the partial trace, observe that they appear in the initial density matrix weighted with

$$e^{-i\phi}\cos^5\left(\frac{\theta}{2}\right)\sin\left(\frac{\theta}{2}\right)\cos^{2k}\left(\frac{\theta}{2}\right)\sin^{2(N-3-k)}\left(\frac{\theta}{2}\right),$$

where k is the number of 0s in $\vec{i}'$ [see Eq. (C1)]. Moreover, after tracing out all spins except the one tagged with $N-1$, there are exactly $C_k^{N-3} = (N-3)!/k!(N-3-k)!$ such factors for each k. Therefore, the total contribution to the operator $|0\rangle\langle 1|$ from the family of operators with the form $|00\vec{i}'0\rangle\langle 10\vec{i}'0|$ is

$$\begin{aligned} e^{-i\phi}\cos^5\left(\frac{\theta}{2}\right)\sin\left(\frac{\theta}{2}\right)\sum_{k=0}^{N-3} C_k^{N-3}\cos^{2k}\left(\frac{\theta}{2}\right)\sin^{2(N-3-k)}\left(\frac{\theta}{2}\right) &= e^{-i\phi}\cos^5\left(\frac{\theta}{2}\right)\sin\left(\frac{\theta}{2}\right)\left[\cos^2\left(\frac{\theta}{2}\right)+\sin^2\left(\frac{\theta}{2}\right)\right]^{N-3} \\ &= e^{-i\phi}\cos^5\left(\frac{\theta}{2}\right)\sin\left(\frac{\theta}{2}\right). \end{aligned} \tag{C2}$$

This result, together with the rest of the cases, is summarized in Table I. Adding up all contributions to the operator $|0\rangle\langle 0|1$, we have (using the notation of Table I)

$$\begin{aligned} [\rho_{N-1}(t)]_{01} &= 2\left(e^{it4J}c_\theta^5 + 2c_\theta^3 s_\theta^2 + e^{-it4J}c_\theta s_\theta^4\right)\frac{e^{-i\phi}s_\theta}{2} \\ &= \gamma(\theta,t)[\rho_{N-1}(0)]_{01}, \end{aligned} \tag{C3}$$

where we have identified $e^{-i\phi}s_\theta/2 = [\rho_{N-1}(0)]_{01}$. The factor $\gamma(\theta,t)$ can be further simplified [see Eq. (47)]. Notice that the result is independent of N.

APPENDIX D: NEGLIGIBILITY OF TERMS IN THE POWER SERIES OF EFFECTIVE ALL-TO-ALL INTERACTION

In Sec. IV, chains evolving due to a nonuniform external magnetic field in the z direction with an all-to-all Ising interaction parallel to the field were considered. By iteratively integrating the Liouville–von Neumann equation, a Dyson series, given by Eq. (38), was obtained. In this series, terms proportional to $\mathcal{C}\{[H_{\rm int}, \varrho_{\max}(0)]\}$ arise, which are discarded. In this Appendix we show that they are in fact negligible.

By virtue of Eq. (9), we know that $\varrho_{\max}(0)$ is of the form $\bigotimes \rho_k$ and so

$$\begin{aligned} \mathcal{C}\{[H_{\rm int}, \varrho_{\max}(0)]\} &= \sum_{k=1}^{N} p_k[\rho_k, \sigma^z]\prod_{j\neq k}\mathrm{tr}(\rho_k\sigma^z) \\ &= \prod_{j=1}^{N}\mathrm{tr}(\rho_j\sigma^z)\sum_{k=1}^{N}\frac{p_k}{\mathrm{tr}(\rho_k\sigma^z)}[\rho_k,\sigma^z], \end{aligned} \tag{D1}$$

TABLE I. Summary of phases gained by each operator type (parametrized by $\vec{i}'$) during microscopic evolution; the $(N-1)$th spin is in bold. The contribution is the sum of all factors that remain once all operators of each family are partially traced (see the main text for details). We use the abbreviations $c_\theta := \cos(\theta/2)$ and $s_\theta := \sin(\theta/2)$.

Operator family	Contribution	Phase
$\|\mathbf{0}0\vec{i}'0\rangle\langle\mathbf{1}0\vec{i}'0\|$	$e^{-i\phi}c_\theta^5 s_\theta$	e^{it4J}
$\|\mathbf{0}0\vec{i}'1\rangle\langle\mathbf{1}0\vec{i}'1\|$	$e^{-i\phi}c_\theta^3 s_\theta^3$	1
$\|\mathbf{0}1\vec{i}'0\rangle\langle\mathbf{1}1\vec{i}'0\|$	$e^{-i\phi}c_\theta^3 s_\theta^3$	1
$\|\mathbf{0}1\vec{i}'1\rangle\langle\mathbf{1}1\vec{i}'1\|$	$e^{-i\phi}c_\theta s_\theta^5$	e^{-it4J}

meaning that

$$\mathcal{C}\{[H_{\text{int}}, \varrho_{\max}(0)]\} \propto \prod_{j=1}^{N} \text{tr}(\rho_j \sigma^z). \tag{D2}$$

The product on the right-hand side of Eq. (D2) is a product of the z components of each subsystem of $\varrho_{\max}(0)$, which we know to be

$$\text{tr}(\rho_j \sigma^z) = \frac{r^z_{\text{eff}}}{r_{\text{eff}}} \tanh(\lambda p_j), \tag{D3}$$

where $r^z_{\text{eff}}/r_{\text{eff}} < 1$. Now, as N grows, $\tanh(\lambda p_j) \approx \lambda p_j$, and if we take p_j of $O(1/N)$, then the product

$$\prod_{j=1}^{N} \text{tr}(\rho_j \sigma^z) = O\left(\frac{1}{N^N}\right), \tag{D4}$$

which implies that

$$\mathcal{C}\{[H_{\text{int}}, \varrho_{\max}(0)]\} = O\left(\frac{1}{N^N}\right), \tag{D5}$$

which decays exponentially as N grows. We conclude that once the coarse-graining map is applied, the odd terms in (39) can be approximated by 0.

[1] J. Kofler and Č. Brukner, Classical world arising out of quantum physics under the restriction of coarse-grained measurements, Phys. Rev. Lett. **99**, 180403 (2007).

[2] S. Raeisi, P. Sekatski, and C. Simon, Coarse graining makes it hard to see micro-macro entanglement, Phys. Rev. Lett. **107**, 250401 (2011).

[3] Ł. Rudnicki, S. P. Walborn, and F. Toscano, Optimal uncertainty relations for extremely coarse-grained measurements, Phys. Rev. A **85**, 042115 (2012).

[4] O. Kabernik, J. Pollack, and A. Singh, Quantum state reduction: Generalized bipartitions from algebras of observables, Phys. Rev. A **101**, 032303 (2020).

[5] M. Gallego and B. Dakić, Macroscopically nonlocal quantum correlations, Phys. Rev. Lett. **127**, 120401 (2021).

[6] A. Alonso-Serrano and M. Visser, Coarse graining Shannon and von Neumann entropies, Entropy **19**, 207 (2017).

[7] M. Radonjić, S. Prvanović, and N. Burić, System of classical nonlinear oscillators as a coarse-grained quantum system, Phys. Rev. A **84**, 022103 (2011).

[8] C. Roh, Y.-D. Yoon, J. Park, and Y.-S. Ra, Continuous-variable nonclassicality certification under coarse-grained measurement, Phys. Rev. Res. **5**, 043057 (2023).

[9] G. D. Carvalho and P. S. Correia, Decay of quantumness in a measurement process: Action of a coarse-graining channel, Phys. Rev. A **102**, 032217 (2020).

[10] S. Mukherjee, A. Rudra, D. Das, S. Mal, and D. Home, Persistence of quantum violation of macrorealism for large spins even under coarsening of measurement times, Phys. Rev. A **100**, 042114 (2019).

[11] T. Heinosaari and M. Ziman, Guide to mathematical concepts of quantum theory, Acta Phys. Slovaca **58**, 487 (2008).

[12] P. Busch and R. Quadt, Concepts of coarse graining in quantum mechanics, Int. J. Theor. Phys. **32**, 2261 (1993).

[13] W. H. Zurek, Decoherence and the transition from quantum to classical, Phys. Today **44**(10), 36 (1991).

[14] M. Schlosshauer, Decoherence, the measurement problem, and interpretations of quantum mechanics, Rev. Mod. Phys. **76**, 1267 (2005).

[15] M. Schlosshauer, Quantum decoherence, Phys. Rep. **831**, 1 (2019).

[16] D. Šafránek, J. M. Deutsch, and A. Aguirre, Quantum coarse-grained entropy and thermodynamics, Phys. Rev. A **99**, 010101(R) (2019).

[17] D. Šafránek, J. M. Deutsch, and A. Aguirre, Quantum coarse-grained entropy and thermalization in closed systems, Phys. Rev. A **99**, 012103 (2019).

[18] C. Duarte, G. D. Carvalho, N. K. Bernardes, and F. de Melo, Emerging dynamics arising from coarse-grained quantum systems, Phys. Rev. A **96**, 032113 (2017).

[19] W. F. Stinespring, Positive functions on C^*-algebras, Proc. Am. Math. Soc. **6**, 211 (1955).

[20] C. Pineda, D. Davalos, C. Viviescas, and A. Rosado, Fuzzy measurements and coarse graining in quantum many-body systems, Phys. Rev. A **104**, 042218 (2021).

[21] A. Einstein, Zur elektrodynamik bewegter körper, Ann. Phys. **322**, 891 (1905).

[22] J. von Neumann, *Mathematical Foundations of Quantum Mechanics* (Princeton University Press, Princeton, 1955).

[23] P. S. Correia, P. C. Obando, R. O. Vallejos, and F. de Melo, Macro-to-micro quantum mapping and the emergence of nonlinearity, Phys. Rev. A **103**, 052210 (2021).

[24] R. O. Vallejos, P. S. Correia, P. C. Obando, N. M. O'Neill, A. B. Tacla, and F. de Melo, Quantum state inference from coarse-grained descriptions: Analysis and an application to quantum thermodynamics, Phys. Rev. A **106**, 012219 (2022).

[25] K. Takasan, K. Adachi, and K. Kawaguchi, Activity-induced ferromagnetism in one-dimensional quantum many-body systems, Phys. Rev. Res. **6**, 023096 (2024).

[26] G. Cho and D. Kim, Machine learning on quantum experimental data toward solving quantum many-body problems, Nat. Commun. **15**, 7552 (2024).

[27] J.-C. Yu, S. Bhave, L. Reeve, B. Song, and U. Schneider, Observing the two-dimensional bose glass in an optical quasicrystal, Nature (London) **633**, 338 (2024).

[28] E. J. Davis, B. Ye, F. Machado, S. A. Meynell, W. Wu, T. Mittiga, W. Schenken, M. Joos, B. Kobrin, Y. Lyu, Z. Wang, D. Bluvstein, S. Choi, C. Zu, A. C. B. Jayich, and N. Y. Yao, Probing many-body dynamics in a two-dimensional dipolar spin ensemble, Nat. Phys. **19**, 836 (2023).

[29] B. Hetényi and J. R. Wootton, Creating entangled logical qubits in the heavy-hex lattice with topological codes, PRX Quantum **5**, 040334 (2024).

[30] C. E. Shannon, A mathematical theory of communication, Bell Syst. Tech. J. **27**, 379 (1948).

[31] E. T. Jaynes, Information theory and statistical mechanics, Phys. Rev. **106**, 620 (1957).

[32] E. T. Jaynes, Information theory and statistical mechanics. II, Phys. Rev. **108**, 171 (1957).
[33] E. H. Wichmann, Density matrices arising from incomplete measurements, J. Math. Phys. **4**, 884 (1963).
[34] M. Ziman, Incomplete quantum process tomography and principle of maximal entropy, Phys. Rev. A **78**, 032118 (2008).
[35] V. Bužek, in *Quantum State Estimation*, edited by M. Paris and J. Řeháček, Lecture Notes in Physics Vol. 649 (Springer, Berlin, 2004), Chap. 6, pp. 189–234.
[36] V. Bužek, G. Drobný, G. Adam, R. Derka, and P. L. Knight, Reconstruction of quantum states of spin systems via the Jaynes principle of maximum entropy, J. Mod. Opt. **44**, 2607 (1997).
[37] F. J. Dyson, The threefold way. Algebraic structure of symmetry groups and ensembles in quantum mechanics, J. Math. Phys. **3**, 1199 (1962).
[38] M. A. Nielsen and I. L. Chuang, *Quantum Computation and Quantum Information*, 2nd ed. (Cambridge University Press, New York, 2000).
[39] M. Žnidarič, C. Pineda, and I. García-Mata, Non-Markovian behavior of small and large complex quantum systems, Phys. Rev. Lett. **107**, 080404 (2011).
[40] H. P. Breuer and F. Petruccione, *The Theory of Open Quantum Systems* (Oxford University Press, Oxford, 2002).
[41] D. Davalos and M. Ziman, Quantum dynamics is not strictly bidivisible, Phys. Rev. Lett. **130**, 080801 (2023).
[42] G. Montes Cabrera, D. Davalos, and T. Gorin, Positivity and complete positivity of differentiable quantum processes, Phys. Lett. A **383**, 2719 (2019).
[43] D. Davalos, M. Ziman, and C. Pineda, Divisibility of qubit channels and dynamical maps, Quantum **3**, 144 (2019).
[44] E.-M. Laine, J. Piilo, and H.-P. Breuer, Measure for the non-Markovianity of quantum processes, Phys. Rev. A **81**, 062115 (2010).
[45] A. Mandilara, J. W. Clark, and M. S. Byrd, Elliptical orbits in the Bloch sphere, J. Opt. B **7**, S277 (2005).
[46] J. A. de Leon, A. Fonseca, F. Leyvraz, D. Davalos, and C. Pineda, Pauli component erasing quantum channels, Phys. Rev. A **106**, 042604 (2022).
[47] L. Li, M. J. W. Hall, and H. M. Wiseman, Concepts of quantum non-Markovianity: A hierarchy, Phys. Rep. **759**, 1 (2018).
[48] A. S. Holevo, *Statistical Structure of Quantum Theory*, Lecture Notes in Physics Monographs Vol. 67 (Springer, Berlin, 2001).
[49] J. Eisert, M. Friesdorf, and C. Gogolin, Quantum many-body systems out of equilibrium, Nat. Phys. **11**, 124 (2015).
[50] A. Kandala, A. Mezzacapo, K. Temme, M. Takita, M. Brink, J. M. Chow, and J. M. Gambetta, Hardware-efficient variational quantum eigensolver for small molecules and quantum magnets, Nature (London) **549**, 242 (2017).
[51] D. Davalos, A. C. Castillo, E. S. Navarrete, and C. Pineda, Zenodo (2025), https://zenodo.org/records/16734705.